Delft University of Technology

Transmission electron imaging in the Delft multibeam scanning electron microscope 1

Ren, Yan; Kruit, Pieter

DOI
10.1116/1.4966216

Publication date
2016

Document Version
Final published version

Published in
Journal of Vacuum Science and Technology B: Nanotechnology and Microelectronics

Citation (APA)
Ren, Y., & Kruit, P. (2016). Transmission electron imaging in the Delft multibeam scanning electron microscope 1. *Journal of Vacuum Science and Technology B: Nanotechnology and Microelectronics*, *34*(6), Article 06KF02. https://doi.org/10.1116/1.4966216

Important note
To cite this publication, please use the final published version (if applicable).
Please check the document version above.

Copyright
Other than for strictly personal use, it is not permitted to download, forward or distribute the text or part of it, without the consent of the author(s) and/or copyright holder(s), unless the work is under an open content license such as Creative Commons.

Takedown policy
Please contact us and provide details if you believe this document breaches copyrights.
We will remove access to the work immediately and investigate your claim.

This work is downloaded from Delft University of Technology.
For technical reasons the number of authors shown on this cover page is limited to a maximum of 10.

.

Transmission electron imaging in the Delft multibeam scanning electron microscope 1

Yan Ren and Pieter Kruit

Citation: Journal of Vacuum Science & Technology B, Nanotechnology and Microelectronics: Materials, Processing, Measurement, and Phenomena **34**, 06KF02 (2016); doi: 10.1116/1.4966216

View online: http://dx.doi.org/10.1116/1.4966216

View Table of Contents: http://avs.scitation.org/toc/jvb/34/6

Published by the American Vacuum Society

Articles you may be interested in

PMMA removal selectivity to polystyrene using dry etch approach
Journal of Vacuum Science & Technology B, Nanotechnology and Microelectronics: Materials, Processing, Measurement, and Phenomena **34**, 061802061802 (2016); 10.1116/1.4964881

Embedded silicon carbide “replicas” patterned by rapid thermal processing of DNA origami on silicon
Journal of Vacuum Science & Technology B, Nanotechnology and Microelectronics: Materials, Processing, Measurement, and Phenomena **34**, 060602060602 (2016); 10.1116/1.4965726

Prediction of surface topography due to finite pixel spacing in FIB milling of rectangular boxes and trenches
Journal of Vacuum Science & Technology B, Nanotechnology and Microelectronics: Materials, Processing, Measurement, and Phenomena **34**, 061803061803 (2016); 10.1116/1.4967249

Electron beam lithography patterned hydrogen silsesquioxane resist as a mandrel for self-aligned double patterning application
Journal of Vacuum Science & Technology B, Nanotechnology and Microelectronics: Materials, Processing, Measurement, and Phenomena **34**, 061601061601 (2016); 10.1116/1.4963194

Instruments for Advanced Science

Contact Hiden Analytical for further details:
W www.HidenAnalytical.com
E info@hiden.co.uk
CLICK TO VIEW our product catalogue

Gas Analysis
- dynamic measurement of reaction gas streams
- catalysis and thermal analysis
- molecular beam studies
- dissolved species probes
- fermentation, environmental and ecological studies

Surface Science
- UHV TPD
- SIMS
- end point detection in ion beam etch
- elemental imaging - surface mapping

Plasma Diagnostics
- plasma source characterization etch and deposition process reaction kinetic studies
- analysis of neutral and radical species

Vacuum Analysis
- partial pressure measurement and control of process gases
- reactive sputter process control
- vacuum diagnostics
- vacuum coating process monitoring

Transmission electron imaging in the Delft multibeam scanning electron microscope 1

Yan Ren[a)] and Pieter Kruit
Department of Imaging Physics, Delft University of Technology, Lorentzweg 1, 2628 CJ Delft, The Netherlands

(Received 24 June 2016; accepted 14 October 2016; published 27 October 2016)

Our group is developing a multibeam scanning electron microscope (SEM) with 196 beams in order to increase the throughput of SEM. Three imaging systems using, respectively, transmission electron detection, secondary electron detection, and backscatter electron detection are designed in order to make it as versatile as a single beam SEM. This paper focuses on the realization of the transmission electron imaging system, which is motivated by biologists' interest in the particular contrast this can give. A thin sample is placed on fluorescent material which converts the transmitted electrons to photons. Then, the 196 photon beams are focused with a large magnification onto a camera via a high quality optical microscope integrated inside the vacuum chamber. Intensities of the transmission beams are retrieved from the camera images and constructed to form each beam's image using an off line image processing program. Experimental results prove the working principle of transmission electron imaging and show that details of 10–20 nm in images of biological specimen are visible. Problems encountered in the results are discussed and plans for future improvements are suggested. © *2016 American Vacuum Society*.
[http://dx.doi.org/10.1116/1.4966216]

I. INTRODUCTION

Increasing the imaging throughput of scanning electron microscopy (SEM) could be of great benefit for some applications, especially in biology. For example, making an image of a complete zebra fish sagittal section at 1.6 nm pixel resolution over an area of 1.5×0.6 mm took four and half days.[1] Acquiring a 3D image of a $400 \times 400 \times 1000\,\mu$m mouse cortical volume, with the typical 4 nm resolution, is estimated to take about 400 days, depending on the detection method applied.[2] It will surely help a lot if this imaging acquisition time of 400 days is reduced to one or two days while still keeping the imaging quality.

Multibeam technology is the only option to achieve this. Several groups are doing these, e.g., Mohammadi-Gheidari and Kruit,[3] D. Zeidler and G. Dellemann,[4] and Enyama *et al.*[5] Some published their experimental results, e.g., Mohammadi-Gheidari *et al.*,[6] and Eberle *et al.*[7] Zeiss also released a commercial multibeam SEM (MBSEM) which has 61 or 91 beams, with secondary electron (SE) detection.

Although SE imaging is popularly used in SEM, it is not favored by biologists who want to get component information from biological specimens. Backscatter electron (BSE) imaging is more attractive to them because it mainly provides component information. SE imaging primarily provides topography information and very weakly reflects the component information by so-called SE2s which are generated by BSE in the interaction volume,[8,9] as shown in Fig. 1.

However, BSE imaging encounters problem when biological tissues are sliced very thin. For good 3D structure reconstruction, the slice needs to be about 30–40 nm thin.[2] The BSE generation is low in such thin slices, as it is linearly proportional to the thickness of the tissue,[8] as in

$$\eta(t) = c(E) N Z^2 \rho t, \tag{1}$$

where η is the BSE generation coefficient, c is a constant for one incident beam energy, N is the number of electrons per unit volume, Z is the atomic number, ρ is the atomic density, and t is the thickness of the tissue. BSE imaging needs a long dwell time to obtain a decent image with such thin samples. Our imaging experience tells us that the dwell time needs 10 μs for landing energy 5 keV using the concentric backscatter detector in FEI Verios SEM when the tissue is not heavily stained.

Transmission electron (TE) imaging offers another possibility to produce good contrast imaging, because the transmission signal, similar to the BSE signal, also carries the composition and mass density information. For very thin tissues, the TE generation coefficient can be estimated as

$$\gamma = 1 - \eta, \tag{2}$$

where γ is the TE generation coefficient. When the sample is very thin, γ usually is much larger than η except when the primary beam's landing energy is so low that most primary electrons are absorbed in the sample. For 10 keV landing energy and a 50 nm biological tissue slice, γ is even $>99\%$.[10] So, it is easier to detect TE than to detect BSE for thin tissue. This does not mean, however, that the TE signal provides better imaging contrast or signal to noise ratio. This is as complicated as comparing bright field imaging to dark field imaging, and is beyond the scope of this paper.

Some researchers have already shown good quality TE imaging results using biological specimens.[10,11] Kuipers *et al.* even proved that TE imaging quality was as good as, or even better than BSE imaging quality in their research.[12] Besides, since the invention of the transmission electron microscope (TEM), biologists have used mainly bright field transmission imaging for their low-to-medium resolution

[a)]Electronic mail: y.ren-1@tudelft.nl

 © 2016 American Vacuum Society

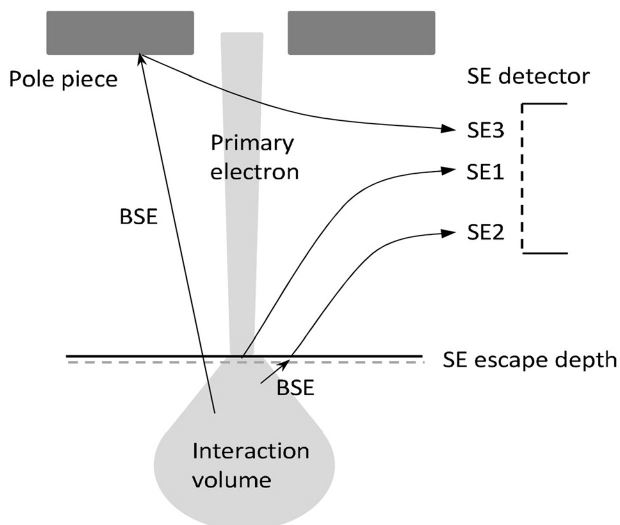

FIG. 1. Illustration of different types of secondary electrons: SE1, SE2, and SE3.

images. Such results have motivated us to develop a TE imaging system in our MBSEM.

In this article, the optical system in our MBSEM (the Delft MBSEM1) is briefly explained; the design principle of TE imaging system in the Delft MBSEM1 is discussed in detail and our first, low throughput experimental results using off line image processing program are presented. Problems encountered in the experiments are discussed, and plans for future improvements are suggested. It is possible to apply the technology used for the TE imaging in the Delft MBSEM to other types of MBSEMs.

II. OPTICAL SYSTEM IN THE DELFT MBSEM1

Figure 2 shows a schematic overview of the electron optical system in the Delft MBSEM1, which is based on a regular FEI Nova-Nano 200 SEM, but equipped with a multielectron beam source (MBS) module. It uses one ZrO/W Schottky source to generate a 14×14 array of focused beams with a resolution and current per beam comparable to a state of the art single beam SEM.[3] So, this MBSEM should have 196 times higher throughput than a single beam SEM if we can make the detection as efficient.

Determined by the MBS unit, the ratio of geometrical spot size of beams over the pitch on the sample is fixed, 95 nm/70 μm. The beams' pitch on the sample is adjustable, but preferably smaller than 5 μm, otherwise off axis aberrations make the outermost off axis beam's spot size much larger than the axial beam's spot size in the simulation using the electron optical design[13] package. In the simulation, we set a criterion that the outermost beam should not be 1.2 times larger than the axial beam in order to keep the beams' uniformity.

A single beam working mode is also available in the Delft MBSEM1.[6] In this mode, instead of all the beams having a crossover in the variable aperture [(VA) shown in Fig. 2], the beams are separate with a pitch larger than the aperture size so that only one beam can go down to scan the sample. The single beam mode works the same way as in the standard single beam SEM. It can be used to get a large field of view (FOV) and to pinpoint the region of interest. Then, the multibeam mode is switched on for high throughput imaging. The mode switch is simply done by assigning magnetic lenses with different strengths.

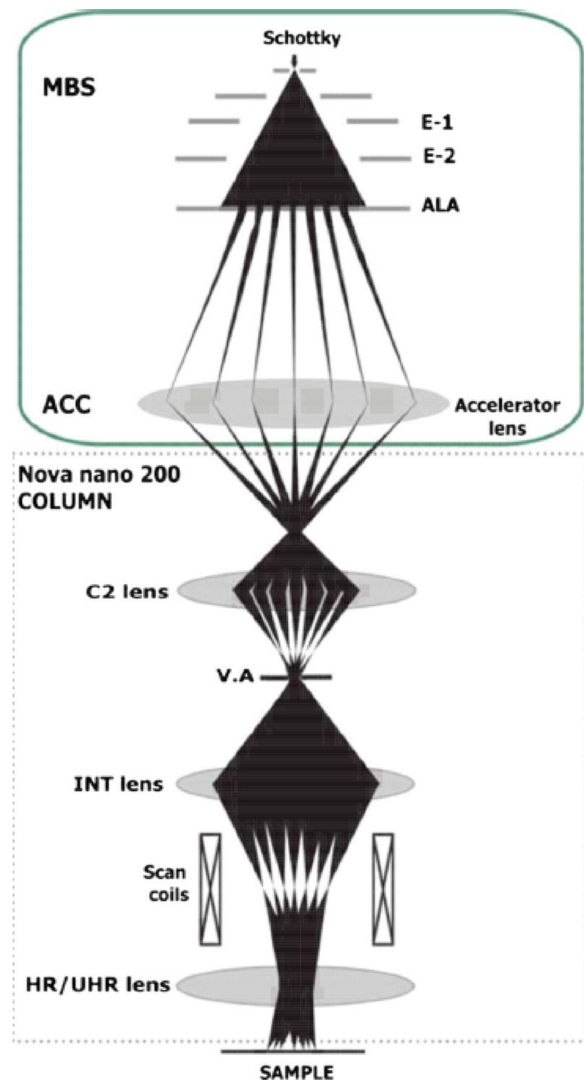

FIG. 2. (Color online) Optics schematic of MBSEM. Multibeam source, electrode 1, electrode 2, aperture lens array, accelerator lens, variable aperture, intermediate lens, high resolution lens and ultrahigh resolution lens are abbreviated as MBS, E-1, E-2, ALA, ACC, INT lens, HR and UHR lens, respectively.

Three imaging systems are planned to be built in this MBSEM: for TE, SE, and BSE detection, respectively.

For SE detection in MBSEM, a new detection strategy should be developed. It is impossible to use the traditional SE detection method employed in single beam SEM because all SE beams are mixed and there is no way to separately collect one beam's SE signal. Generally speaking, in MBSEM, the SE beams generated on sample need to be accelerated into the SEM column, and to be focused with a large magnification in a chosen detection plane to make SE beams' pitch larger than SE beams' spot size so that SE beams can be separately collected. Meanwhile, the primary

beams' focusing will be modified but should not be disturbed by the SE beams' focusing and detection. In the Delft MBSEM1, it is preferable to place the SE detector in a plane (such as the VA plane) where the primary beams have a common crossover in order to make the SE detection bring as little disturbance as possible to the primary beams and to keep the whole system compact. An electrostatic lens is introduced to generate proper energy difference between the primary beams and the SE beams, the difference which makes it possible to use the same lenses to focus the primary beams on the sample and to focus the SE beams in the detection plane. Some mechanical modification has to be done to achieve the SE detection. The methods used in the Delft MBSEM1 will be reported in a separate paper.

The BSE detection in MBSEM is more difficult than the SE detection. In the conventional definition, BSE has an energy range from 50 eV to the primary beam's energy with a full opening angle (from 0° to 90°). Such distribution makes it very hard to separate one beam's BSE signal from its neighbors'. We are struggling to find a good solution and as far as we know, no BSE detection system has yet been successfully developed for MBSEM.

TE imaging does not need any modification to the primary beams' focusing setup. This advantage makes it possible to apply the TE imaging system to every MBSEM. This paper focuses on the realization of TE imaging in the Delft MBSEM1.

III. TE IMAGING SYSTEM DESIGN IN DELFT MBSEM1

The first challenge of the TE detection is to separately collect the TE signals because they have the same small pitch as the primary beams have on the sample, smaller than 5 μm, even smaller than 1 μm for 1.2 nm imaging resolution.[3]

There are at least two ways to do this. The first way is to introduce an additional electron optical system to focus the TE beams with a large magnification onto a detector where the TE beams will be focused with a small spot size and large pitch (at least larger than the largest spot size of focused TE beams). TEM uses this strategy.[14] In TEM, there is no problem getting good focusing with large magnification and one is free to choose between the bright field mode and the dark field mode for different contrast. However, the disadvantage of utilizing this strategy in the MBSEM is that new electron optical lenses need to be added. First, the sample chamber has a finite volume so that it is not easy to insert new electron optical parts, including all the lenses, cables, and connections. Second, the magnetic immersion objective lens which is used to get the best resolution for the primary beams focusing would interfere with the new add-on lenses. Such an objective lens usually has strong excitation and a very long tail.[15] A little change of objective lens excitation may spoil the add-on electron optical system. The combination of these two issues makes it difficult to implement this strategy in this MBSEM.

The other way circumvents the interference issue by converting electrons to photons using fluorescent material. When the TE beam's pitch is larger than the photon generation volume size in the fluorescent material, the 196 separate TE beams create 196 separate light sources. An optical microscope is then used to image these light sources with a large magnification onto a camera. This optical microscope should be capable of working inside the vacuum, providing better resolution than the beams' pitch, providing a large numerical aperture (NA) for a high collection efficiency, and having good alignment with the SEM column. The difficulty of this strategy is in adding such an optical microscope into the SEM's sample chamber. In our group, we had just developed such a platform for correlative light-electron microscopy, the "SECOM platform,"[16] further commercialized by Delmic, a spinoff company in the Netherlands. This platform places the optical microscope inside the vacuum chamber, shown in Fig. 3, and uses the vacuum glass window to transit light between the air environment and the vacuum chamber. It is designed for biological research. Here, we employ this SECOM platform for TE imaging, as schematically shown in Fig. 4.

This strategy has limitations. One limitation is the resolution of optical microscopes. Due to the diffraction limitation, submicrometer resolution is difficult to achieve unless we use liquid immersion lenses. This strategy probably will fail when the primary beams' pitch on the sample is smaller than 1 μm. In terms of resolution, a larger than 1 μm pitch on the sample leads to no better than 3 nm optical imaging resolution of the Delft MBSEM1 because the ratio of geometrical spot size of beams over pitch on the sample is fixed, 95 nm/70 μm.

Another limitation is that the sample should be closely placed on the fluorescent material. When there is a 1 mm gap between the sample and the fluorescent material, if we assume that TE beams have a similar opening angle as the

Fig. 3. (Color) View of integrated optical microscope in SEM chamber.

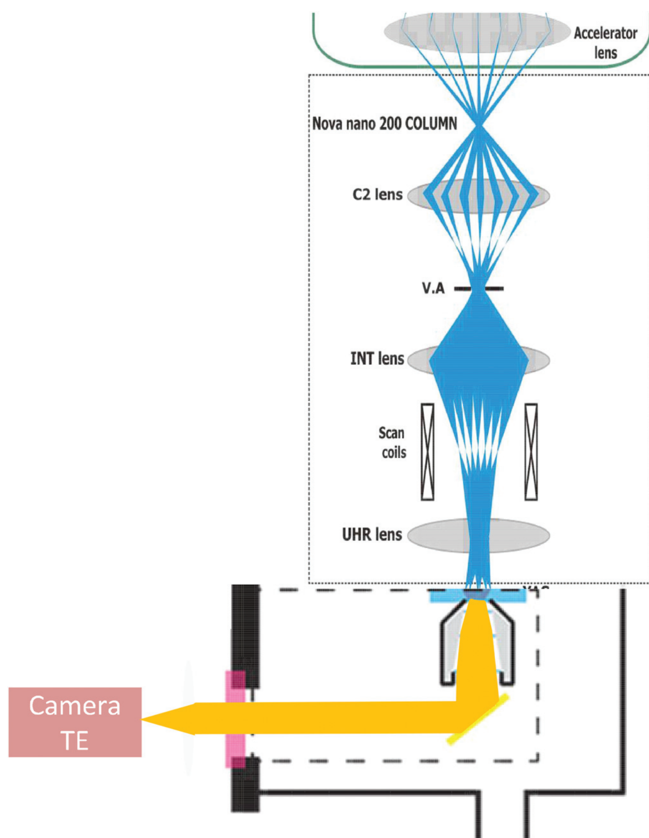

FIG. 4. (Color) Combination of Delft MBSEM1 and SECOM platform.

primary beams, typically 10 mrad, a TE beam grows to be a spot of 20 μm, much larger than the pitch. Neighboring TE beams will mix together in the fluorescent material. So, it is recommended that thin tissue will be directly placed on the fluorescence material to restrain TE beams' spread. The consequence of this placement is that there is no bright field mode and dark field mode anymore in this TE imaging system because all of the transmitted electrons from a primary beam have been collected. Additionally, it will be difficult to remove thin tissues from the fluorescent material without damage.

After comparing these two options, the latter was chosen, that of using the SECOM platform.

The remaining challenge is to detect the intensities of the TE beams. We want to read each beam's TE signal out in each scan step for live imaging. One possible way is to use a detector array, one detector for one beam. This concept is employed in the Zeiss' MBSEM for SE detection and is quite a straightforward method. In the scanning, one beam's signal should always fall into its own detector. Considering that the scanning FOV is usually equal to or a bit larger than the beam's pitch, it is necessary to have descan system which is synchronized with the primary beam deflectors to compensate the TE signal shift on the detector.

It is also possible to use a CCD or CMOS camera and fast image processing technology to detect the intensities. A camera image of the 196 light sources (or the 196 TE beams) is generated in each scan step, an example of which is shown in Fig. 5. These 196 beams' intensities can be retrieved from

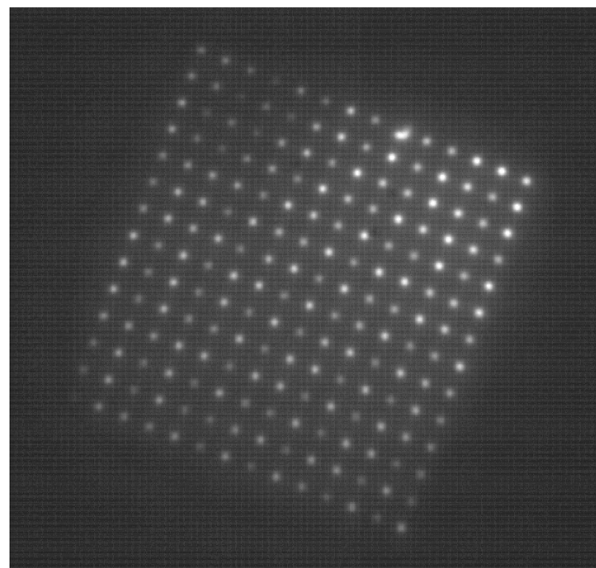

FIG. 5. Image of 196 beams with pitch 4 μm onto an YAG ($Y_3Al_5O_{12}$) screen and recorded by a camera.

such an image and assigned to corresponding beams using an image processing program. For live imaging, these two steps need to done in one scan dwell time.

The advantage of the first option is that each subdetector is similar to a normal detector; so, it is easy to process detected signals. The disadvantages are that we need to add a descan system, and that thousands of electronic cables and controls need to be used for detector array. Plenty of modifications have to be made to the SEM column for this option to be viable.

The advantage of the second option is that it is easy to start because all parts are commercially available for the concept proof test, and the whole detection unit is compact. A disadvantage is that it is very demanding for the camera and the image processing program. If 100 ns dwell time is used—the dwell time which is normally used in single beam SEM for fast scanning—the camera needs to have 10×10^6 frames per second (FPS) rate and very good sensitivity. If one TE spot needs 10×10 camera pixels to record, then there should be more than 19 600 pixels in one camera image. The first problem is that such a camera is both rare and expensive. The second problem is that of transferring and processing 196 GByte data in one second when each pixel has 8 bit depth.

It is hard to tell which one is better, or easier for the TE detection in the Delft MBSEM1. We have chosen an easy start: the combination of a camera and fast image processing technology to prove the working principle of the TE detection system. It is not necessary to use a 10M FPS camera in the beginning stage because it is expensive and complicated to transfer data and process the images so rapidly. We divide the TE imaging system development into three steps. In the first step, off-line image processing with the low throughput imaging method is employed to prove this imaging concept. The camera "Prosilica GE680" from Allied Vision Tech is utilized. It has 7.4 μm pixel size and 205 frames per second

at a resolution of 640 × 480. A Nikon 40× objective lens is used in the optical microscope to have a 40 times magnification. A camera image with 196 TE beams information is saved into a computer in each scan step during a scan period. Then, the off-line image processing program is used to calculate each beam's intensity and position in each scan step and then use all the intensities in a scan period to construct its TE image and the whole TE image map. The experimental results shown in Sec. IV of this paper were obtained using this off-line method.

In the second step, a slow real time imaging program based on field programmable gate arrays (FPGA) technology is developed.[17] A FPGA stands between the camera and the computer. The camera continuously sends images via a camera link to the FPGA where an image processing algorithm is written to calculate each beam's intensity in each scan step. The algorithm builds a beams' mask based on one TE beam's image before the real time imaging starts. In the real time imaging, the mask shifts, synchronized with the beams' scan step, and is used to calculate the beams' intensities quickly in each scan step and to assign intensities to the 196 beams. Then, the FPGA sends these intensities' information to the computer where a Labview program is used to construct TE images. The goal of this step is to achieve a slow real time imaging at a camera rate of several thousand frames per second. In the final step, the fast real time imaging will be realized by utilizing a very fast camera (such as the 10M FPS camera).

To sum up, the TE imaging system of the Delft MBSEM1 adopts a SECOM platform with fluorescent material to convert electrons to photons, a camera, and fast image processing technology. Section IV presents experimental results from off-line processing.

IV. EXPERIMENTAL RESULTS

In the experiment, yttrium aluminum garnet [(YAG), $Y_3Al_5O_{12}$] is chosen to convert electrons to photons, because it has a very high conversion efficiency (about 21 photons/keV/electron for low beam energy) and short decay time (70 ns, which is short enough for our current experiments), in addition to being commercially available in different sizes and thicknesses. Our YAG with a thickness of 20 μm and also the source of the YAG data are supplied by the company "Crytur."

A. Sample information

In the experiments, two types of samples are used. One is a calibration sample, shown in Fig. 6. These patterns are made by depositing tungsten on top of YAG. The line patterns have 1 μm pitch and 0.5 μm line width, and the hole patterns have 0.6 μm pitch and 0.4 μm diameter. The reason to use this calibration sample is that in the Delft MBSEM1, though using the original FEI column, the focusing condition and the lens combinations are different than in the original FEI setup. Thus, scan FOV and magnification shown in FEI user interface are not correct. This sample can be used to calibrate scan FOV.

Fig. 6. (Color online) Calibration sample: the color part is electron transparent area and the white is tungsten. Lines: 0.5 μm wide, 1 μm pitch; holes: 0.4 μm diameter, 0.6 μm pitch.

The other type is rat pancreas tissue provided by UMCG Groningen (Giepmans group) in the Netherlands. The heavily stained sample has a thickness of 100 nm. These samples are directly placed on top of a YAG disk which has 50 nm aluminum coating for conduction and for reflecting all photons to the optical microscope. Although in principle TE imaging is capable of getting good contrast images with little or no stained sample, here the heavily stained sample is used in the experiments. The reason is that the detection chain in the TE imaging system in the Delft MBSEM1 is still in its first development phase and many factors have influence on the TE imaging detection efficiency and the imaging

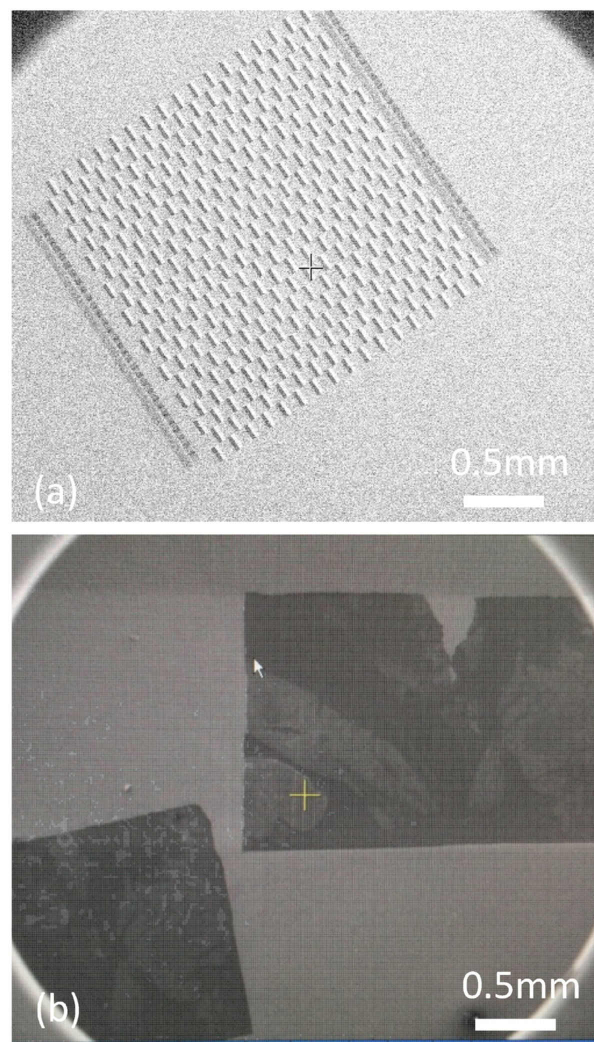

Fig. 7. (Color online) Overview of the samples using single beam mode in order to select region of interest quickly. (a) The calibration sample; (b) the biological sample.

contrast, for example, the choices of camera and fluorescent material, and even the way we prepare the tissues on YAG. Now, we are struggling to find the proper way to place thin tissues on the YAG. So, it is better to start from the sample which is heavily stained and can easily give good contrast images in order to prove the working principle.

B. Imaging results in Delft MBSEM1

All the experiments in this section are done using a landing energy of 15 keV in the Delft MBSEM1.

1. Single beam mode imaging

In the operation, it is preferable to use single beam mode to have an overview of the sample and then to select the region of interest (Fig. 7).

2. Multibeam mode imaging

The 196 beams are labeled by using four quadrants, shown in Fig. 8. Beams from different locations in the E-beam grid give similar performance using the calibration sample, shown in Fig. 9. These images are used to calibrate the scan FOV and scan magnification.

Figures 10 and 11 show TE images of the rat pancreas tissue sample. The beams, regardless of whether from the center or from the edge of the E-beam grid, give quite an even imaging quality.

The image map is constructed by stitching the 196 TE images. In this process, beams' scan direction needs to be parallel with one side of E-beam grid. In principle, the scan FOV can be equal to the pitch of the E-beam grid on the sample so that no stitching program is needed afterward, which is our goal. Then, the beam scan direction and scan FOV need to be accurately set. This can be done after several attempts on a certain working condition and will easily be done when real time imaging is available. Currently, however, it takes too much time because off-line image processing is used. In this stage, it is not necessary because we just intend to prove the working concept, not to deliver the perfect image map which is the goal of our imaging system in the future. Now we align the scan direction with the E-beam grid coarsely and set scan FOV to 10%–20% larger than the pitch of the E-beams on the sample, and then construct an image map using a stitching software called "TRAKEM2."[18] In this way, the beams' images may show slight rotation with respect to the beam array in the image map because the scan direction is not accurately aligned with one side of the E-beam grid on the sample. This is demonstrated in

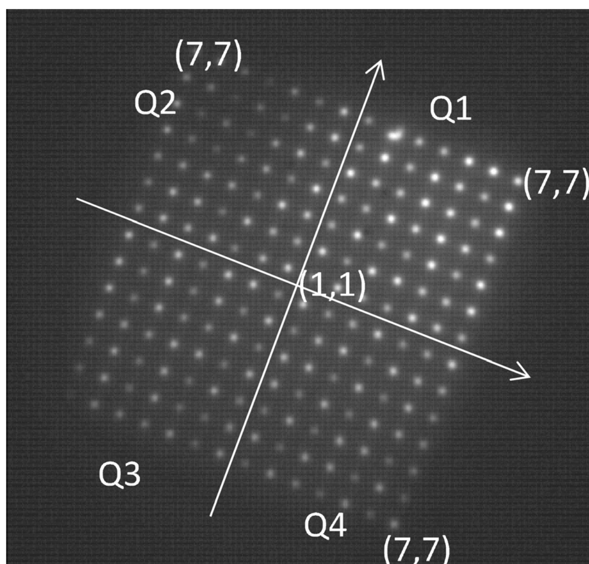

Fig. 8. Beams are labeled by four quadrants in the grid.

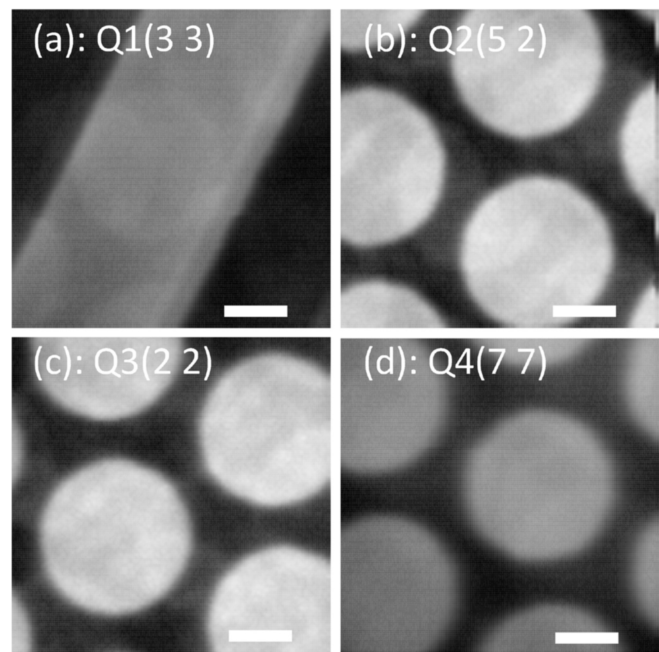

Fig. 9. Different beam's TE image using calibration sample. They are captured simultaneously and their FOV of images is 1.0 μm. Scale bars 200 nm.

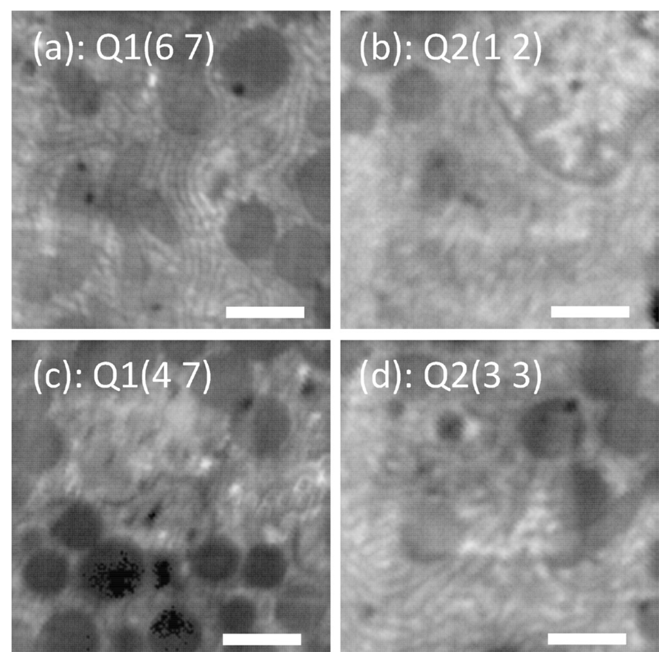

Fig. 10. Different beams' TE images using pancreas tissue captured simultaneously; they have FOV 4.0 μm with 20 nm pixel size. Scale bars 1 μm.

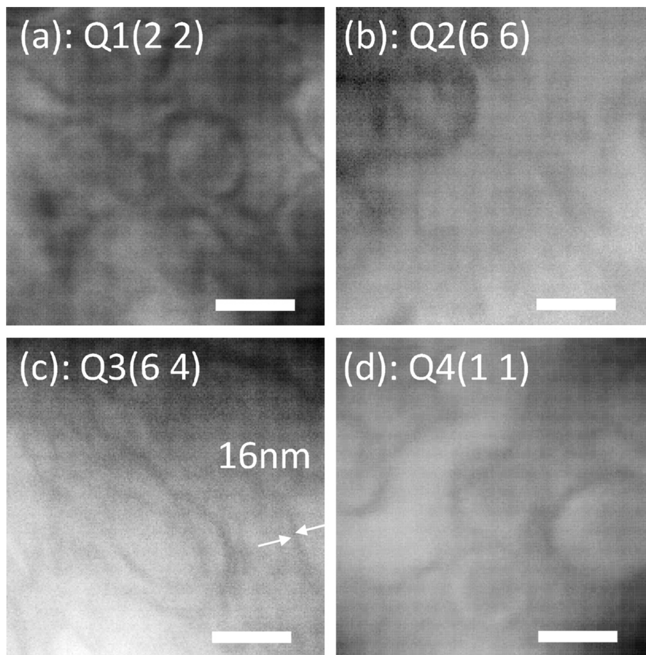

FIG. 11. Different beams' TE images using pancreas tissue recaptured simultaneously; they have FOV 0.8 μm with 4 nm pixel size; details of 10–20 nm are visible in these images. Scale bars 200 nm.

Figs. 12 and 13 which show image maps with 25 and 50 μm FOV, acquired by using different E-beam grid pitches on the sample. No stitching is applied in these two figures. This scan direction misalignment shows more clearly in the image map after stitching. In the stitching, the subimage overlap is set, and the linear blending fusion method embedded in the TrackEM2 is applied. The image map seems tilted at a small angle, leaving some dark areas near the boundary of the image

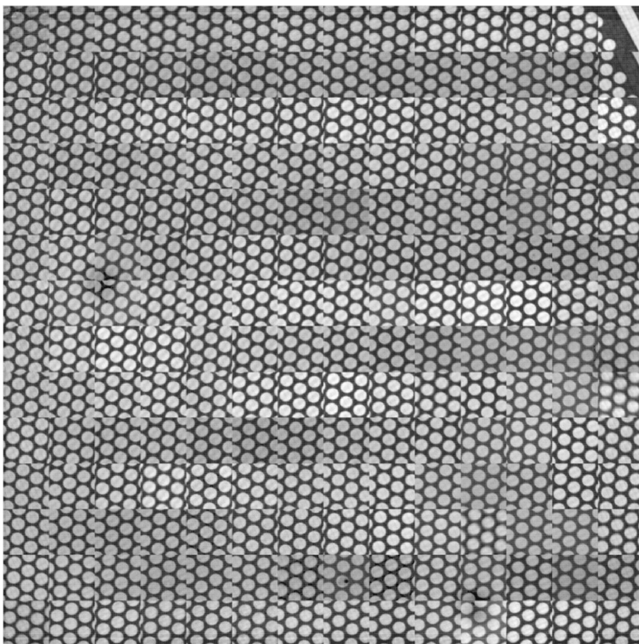

FIG. 12. TE image map of calibration sample formed by 14 × 14 subimages using Delft MBSEM1, without stitching, FOV 25 μm with 2800 × 2800 pixels.

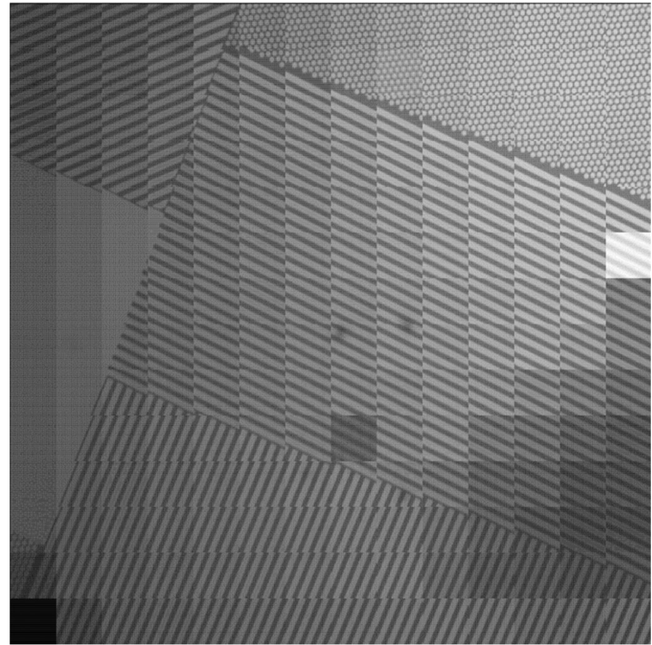

FIG. 13. TE image of calibration sample formed by 14 × 14 subimages using Delft MBSEM1, without stitching, FOV 50 μm with 2100 × 2100 pixels.

map frame, as in Figs. 14 and 15, which show image maps of biological tissue after stitching, with FOV 50 μm with 2600 × 2500 pixels. Figure 14 has more misalignment between beams' scan direction and one side of the E-beam grid; so, its image map has a larger dark area near the frame boundary.

V. DISCUSSION

A. Present imaging speed and image size

In this paper, these results are used to demonstrate the principle of TE imaging. It now takes us about 20 min to

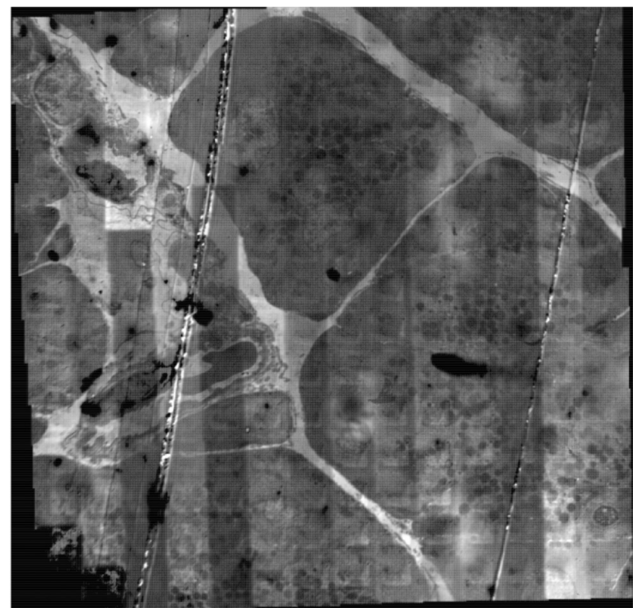

FIG. 14. TE image map 1 of pancreas tissue formed by 14 × 14 subimages using our MBSEM, FOV 50 μm with 2600 × 2500 pixels. Subimages are stitched using the software TRAKEM2.

FIG. 15. TE image map 2 of pancreas tissue formed by 14×14 subimages using our MBSEM, FOV 50 μm with 2600×2500 pixels. Subimages are stitched using the software TRAKEM2.

finish one TE image map. The image maps with FOV 50 μm have 2600×2500 pixels. The pixel size in the image maps is around 20 nm. Clearly, this is not yet high resolution and high throughput imaging. The following paragraphs explain briefly why we cannot achieve high resolution and high throughput imaging yet in our MBSEM.

The GE680 camera is not very fast, just 240 FPS when the camera delivers an image of 400×400 pixels. When the beams' scan resolution is 200×200, it takes this camera 3 min. The image processing program takes about 17 min to analyze camera images and to construct TE images. These make the imaging speed low in the TE imaging system in the Delft MBSEM1, unsurprising considering that the off-line processing mode is used.

In each scan step, the useful information that we really want is the 196 beams' intensities and positions. It is 588 Byte if each parameter takes 1 byte to record. However, in the off-line processing mode, the camera sends an image with 400×400 pixels with 8 bit depth to the computer. This is 160 kByte, 271 times more than what we need. If the beams' scan resolution is 200×200, the camera will generate 6.4 GByte data in one scan period although the useful information is just 23.5 Mbyte. Our current test program, based on LabVIEW, is capable of handling no more than 8 GByte data in one scan period. So, the scan resolution cannot be set to be 500×500 if a camera image still has 400×400 pixels. This limited scan resolution makes large pixel size or scan step size in TE images even larger than the primary beam's spot size on the sample. For example, when a beam's scan FOV is 4 μm, each scan step is 20 nm using 200×200 scan resolution, while the expected primary beam resolution is about 12 nm calculated in the simulation. The camera and the test program limit the size and imaging resolution in the image maps.

This low imaging throughput and small image size will be improved in the planned TE imaging system development. For example, in the second step, a faster camera, the Optronis CL600 × 2 CMOS, is used, which has 2000 FPS when each camera image has 512×512 pixels. Additionally, FPGA is used to process images much more rapidly. It is able to send 5.4 Gbyte per second from the CL600 × 2 camera to the frame grabber with on board FPGA (NI PCIe-1473R) via the FPGA camera link. The FPGA processes the camera images to generate the 196 beams' intensities and positions, and sends this useful information to a computer where TE images are constructed. Then, it will take about 20 s—instead of 20 min—to finish the image maps we had now, 60 times faster. The imaging throughput in the Delft MBSEM1 will then be higher than that of a single beam SEM, but still lower than that of the commercial MBSEM. However, it will allow a scan step smaller than the expected size of the primary beams so that the resolution can be measured and optimized. After the third development step, the fast real time imaging will be available and the Delft MBSEM1 should deliver the high resolution and high throughput TE imaging.

Although such limitations exist in our current imaging system, this test Labview program is already able to check fine features of the samples by setting a small FOV (smaller than the TE beams pitch on the sample). Figure 11 shows four TE images with FOV 0.8 μm and examples of 400×400 scan resolution while the pitch of E-beam grid on the sample is 1.8 μm. The details of 10–20 nm size can be seen in these images. It would be premature at this time to state our MBSEM's imaging resolution because biological tissue itself and these images are not suitable for evaluating imaging resolution. Although we tried to deposit gold particles (the mixture of 5 nm gold particles, 15 nm gold particles, and 50 nm gold particles) on a YAG disk to test resolution, the gold particles clustered together and it was not possible to test resolution at all. A special resolution test sample is needed to test resolution in this TE imaging system, for example, line or dots patterns with the size of a few nanometers deposited on YAG using electron beam induced deposition or similar microelectromechanical systems technology.

B. Intensity differences in image map

There are quite clear intensity differences among neighboring subimages in the image maps. The possible causes of this nonuniformity are as follows:

(1) Different beams' currents due to contamination in the aperture lens array (ALA) which splits the original beam into multiple beams. This would not be surprising after five years of using the same aperture plate.
(2) Misalignment in the MBSEM column, resulting in different beams being differently aligned on the variable aperture, thus selecting different currents.
(3) Some imperfection in the detection chain and the image processing.

The first cause has already been proved by checking a sample without any pattern, such as pure YAG. When all

primary beams come down to that sample without using any aperture in the column, quite a few beams' profiles are not round any more, but with irregular shapes. This tells us that some apertures of the ALA in the MBS are contaminated. This contamination needs to be verified by using a standard SEM. However, in order to take the aperture array out, the whole MBS needs to be disassembled. The MBSEM needs to be shut down at least for one month. This verification was subsequently postponed until the time that the emission tip needs to be replaced.

The primary beams have a common crossover in the variable aperture plane so that apertures here are used to choose different currents. Because of the spherical aberration in the accelerator (ACC) lens (in this paper, only the ACC lens is used to form the common crossover and the C2 lens is off), the off axis beams are shifted a bit away from the axis. After the variable aperture, the central portion of the axial beam is selected, but a different portion of the off axis beams is selected. Once the electron optics is fixed, these selections really depend on the position of the variable aperture. The misalignment, together with contamination in the aperture array, makes the current selection for off axis beams a bit unpredictable.

The optical microscope may make the off axis beams lose more photons than the axial beam. The uniformity of the camera pixels' output and the image processing program may also introduce some intensity difference even when the electron optical side is perfect. So, an intensity match program is needed to eliminate or greatly reduce this nonuniform intensity inside the image map in the future.

C. Crosstalk influence

Figure 16 shows the line profiles in two E-beam grids. It is obvious that there is a crosstalk among neighboring beams even at 4 μm pitch. However, we cannot see the crosstalk effect contribution in sub-beam images. So, in this paper, we neglect the crosstalk influence, but we believe that when the e-beam grid pitch becomes close to the size of one beam inside the YAG, this influence will be problematic.

This crosstalk effect can be measured. For example, a single beam SEM and the Delft MBSEM1 image the same area in a sample using the same detection system. The single beam SEM image has the real sample information. The MBSEM image has the real sample information plus the crosstalk influence. Each pixel's intensity in the MBSEM image minus the corresponding pixel's intensity in single beam SEM image reveals the crosstalk influence. The deterioration of the imaging quality due to the crosstalk effect should be analyzed based on specific application.

D. Subimage boundary in image map

Some subimages' boundaries are apparent in the image maps, as can be seen in Figs. 14 and 15, even after different diffusion methods (such as linear blending, average, median, max intensity, etc.) are tried in the TRAKEM2. This is a common but very tough challenge in the stitching. So far, it is popular to use automatic stitching with the help of manual

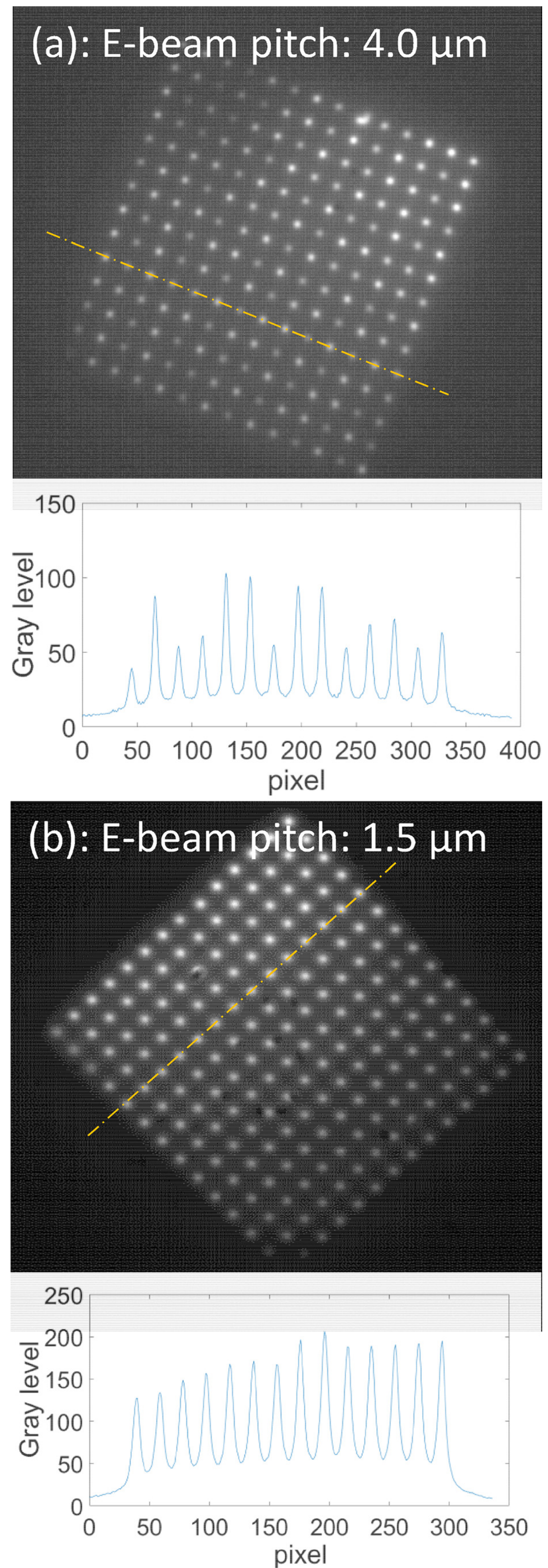

FIG. 16. (Color online) Line profiles in E-beam grid with 4 μm pitch and 1.5 μm pitch. In (a), there are patterns on the YAG; in (b) there is no pattern on the YAG.

stitching in the construction of image maps. However, as there are 196 subimages generated in this MBSEM in one scan period, it is hardly possible to do manual stitching. A good automatic stitching program is expected to take a long calculation time. Meanwhile, we can make improvements by aligning the scan direction well with the e-beam grid direction and matching the scan FOV well with e-beam grid pitch.

VI. CONCLUSION AND OUTLOOK

This article provides one method to achieve TE imaging in the Delft MBSEM1. In this image system, YAG is adopted to convert the 196 TE beams to 196 photon beams; an optical microscope with high NA and good alignment with the electron optical axis is used inside the sample chamber to focus the 196 photon beams on to a camera with large magnification. An off line image processing program is used to retrieve each beam's transmission signal and construct images. A calibration sample and biological tissues are imaged to prove the working principle of this method.

Limited by the camera and the test Labview program, the imaging throughput is low, approximately 20 min to finish images of one scan period with low scan resolution (200×200). Our second step of TE imaging system development is underway and should deliver relatively fast (a few thousand scan steps per second) real time imaging with a faster CMOS camera "Optronis CL600 $\times$ 2" and a FPGA based image processing program. Our ultimate goal is to achieve rapid (100 ns scan dwell time) real time imaging using a super-fast camera (at least with 10M FPS).

In the second and third development steps, the whole detection chain also needs to be optimized, such as the choices of the camera and the fluorescent material, the way to prepare the sample in the TE imaging system in the Delft MBSEM1, etc. The study of the imaging properties, including the image contrast, the detection quantum efficiency, and the optimum imaging throughput, needs to be carried on when the real time imaging is available.

The imaging resolution of TE images from the Delft MBSEM has not yet been measured because the proper resolution test sample needs to be prepared, preferably having a few nanometer scale patterns on a fluorescent material, but the details of 10–20 nm in images of biological specimen are visible in the TE images. The intensity difference in the image maps is clearly shown in the image maps. In the future, elements such as the aperture array, the electron optics alignment, and image processing program need to be checked for correction. The crosstalk among neighboring beams in the E-beam grid is found in the experiments but is not clearly shown in the TE images. When the pitch of E-beam grid on the sample is close to the size of one beam in the YAG, it will give problems. Its influence in TE images should be analyzed in the future. A good stitching program and/or good control of the beam scan direction and scan FOV will be helpful in eliminating the subimages' boundary in the image map.

ACKNOWLEDGMENTS

The authors acknowledge Jacob Hoogenboom for advice on biological imaging, Kees Hagen for discussions, Christiaan Zonnevylle for help with the SECOM platform and discussion on TE imaging system buildup, Ben Giepmans' group for biological tissue preparation, and Thomas Verduin, Paul Keijzer, Wilco Zuidema, and Lennard Voortman for assistance with the image processing program.

[1]F. G. Faas, M. C. Avramut, B. M. van den Berg, A. M. Mommaas, A. J. Koster, and R. B. Ravelli, J. Cell Biol. **198**, 457 (2012).
[2]K. L. Briggman and D. D. Bock, Curr. Opin. Neurobiol. **22**, 154 (2012).
[3]A. Mohammadi-Gheidari and P. Kruit, Nucl. Instrum. Methods A **645**, 60 (2011).
[4]V. Marx, Nature **503**, 147 (2013).
[5]M. Enyama, M. Sakakibara, S. Tanimoto, and H. Ohta, J. Vac. Sci. Technol., B **32**, 051801 (2014).
[6]A. Mohammadi-Gheidari, C. W. Hagen, and P. Kruit, J. Vac. Sci. Technol., B **28**, C6G5 (2010).
[7]A. L. Eberle, S. Mikula, R. Schalek, J. Lichtman, M. L. K. Tate, and D. Zeidler, J. Microsc. **259**, 114 (2015).
[8]L. Reimer, *Scanning Electron Microscopy: Physics of Image Formation and Microanalysis* (Springer, Verlag, Berlin, Heidelberg, 1998).
[9]J. Cazaux, J. Microsc. **214**, 341 (2004).
[10]A. Takaoka and T. Hasegawa, J. Electron Microsc. **55**, 157 (2006).
[11]P. G. Merli and V. Morandi, Microsc. Microanal. **11**, 97 (2005).
[12]J. Kuipers, P. de Boer, and B. N. G. Giepmans, Exp. Cell Res. **337**, 202 (2015).
[13]B. Lencova and J. Zlamal, Electron Optical Design program package EOD3.069, 2006.
[14]L. Reimer, *Transmission Electron Microscopy: Physics of Image Formation and Microanalysis* (Springer, Verlag, Berlin, Heidelberg, 1997).
[15]J. Orloff, *Handbook of Charged Particle Optics* (CRC, Boca Raton, 1997).
[16]A. C. Zonnevylle, R. F. C. Van Tol, N. Liv, A. C. Narvaez, A. P. J. Effting, P. Kruit, and J. P. Hoogenboom, J. Microsc. **252**, 58 (2013).
[17]S. Rahangdale, P. Keijzer, and P. Kruit, *2016 International Conference on Systems, Signals and Image Processing (IWSSIP)* (2016).
[18]A. Cardona and S. Saalfeld, TRAKEM2 v. 1.0c, ImageJ, 2014.